Characterization of Respiratory Drug Delivery with Enhanced Condensational Growth using an Individual Path Model of the Entire Tracheobronchial Airways

Geng Tian[1], **Philip Worth Longest**[1,2], **Guoguang Su**[1], and **Michael Hindle**[2]

[1]Department of Mechanical Engineering, Virginia Commonwealth University, 401 West Main Street, P.O. Box 843015, Richmond, VA 23284-3015, USA

[2]Department of Pharmaceutics, Virginia Commonwealth University, Richmond, VA, USA

Abstract

The objective of this study was to evaluate the delivery of inhaled pharmaceutical aerosols using an enhanced condensational growth (ECG) approach in an airway model extending from the oral cavity to the end of the tracheobronchial (TB) region. The geometry consisted of an elliptical mouth-throat (MT) model, the upper TB airways extending to bifurcation B3, and a subsequent individual path model entering the right lower lobe of the lung. Submicrometer monodisperse aerosols with diameters of 560 and 900 nm were delivered to the mouth inlet under control (25 °C with subsaturated air) or ECG (39 or 42 °C with saturated air) conditions. Flow fields and droplet characteristics were simulated using a computational fluid dynamics model that was previously demonstrated to accurately predict aerosol size growth and deposition. Results indicated that both the control and ECG delivery cases produced very little deposition in the MT and upper TB model (approximately 1%). Under ECG delivery conditions, large size increases of the aerosol droplets were observed resulting in mass median aerodynamic diameters of 2.4–3.3 μm exiting B5. This increase in aerosol size produced an order of magnitude increase in aerosol deposition within the TB airways compared with the controls, with TB deposition efficiencies of approximately 32–46% for ECG conditions. Estimates of downstream pulmonary deposition indicted near full lung retention of the aerosol during ECG delivery. Furthermore, targeting the region of TB deposition by controlling the inlet temperature conditions and initial aerosol size also appeared possible.

Keywords

Respiratory drug delivery; Nanoaerosols; Hygroscopic droplet growth; CFD modeling; Individual path airway model; Targeted aerosol deposition

INTRODUCTION

The delivery of inhaled medicines to the lungs is known to be highly inefficient due to large depositional losses in the delivery device and complex extrathoracic anatomy.[4,5,13,49] Available aerosol delivery devices including pressurized metered dose inhalers (MDI), dry powder inhalers (DPI), nebulizers, and softmist platforms currently have lung delivery efficiencies in the range of 5–70%.[9,28,44,62] Low lung delivery has been shown to correlate

Address correspondence to Philip Worth Longest, Department of Mechanical Engineering, Virginia Commonwealth University, 401 West Main Street, P.O. Box 843015, Richmond, VA 23284-3015, USA. pwlongest@vcu.edu.

with high dose to dose variability,[4] leading to increased side effects and decreased drug effectiveness. To improve penetration of the inhaled medicines to the lungs, inhaled nanoaerosols in the size range of 40–1000 nm are reported to significantly reduce device and extrathoracic deposition.[7,55] Pharmaceutical nanoaerosols have also been suggested for therapeutic applications due to altered monocyte recruitment, large surface area, the ability to penetrate the mucus layer, and rapid drug dissolution and uptake properties.[3,24,51] However, aerosols that are inhaled in the size range of 40–1000 nm lack a strong mechanism for effective deposition in the lungs and are easily exhaled.[20]

Enhanced condensational growth (ECG) is a recently proposed respiratory drug delivery approach that is intended to significantly improve the lung deposition efficiency of pharmaceutical aerosols and to provide full lung retention of inhaled nanoaerosols.[17,29,38] In this approach, a submicrometer or nanometer scale aerosol is delivered to the respiratory airways in conjunction with an airstream that is saturated or supersaturated with water vapor and above body temperature. Aerosols in the size range of 100–1000 nm are considered in order to minimize deposition in the extrathoracic airways and maximize the dose of delivered drug. As a result, aerosol depositional loss in the delivery device and MT or nasal region are largely eliminated. The inhaled water vapor is used to create supersaturated conditions within the respiratory airways. Submicrometer droplets in this supersaturated environment increase in size at a controlled rate due to condensation. Size increase to within the range of 2–3 μm is used to ensure deposition and full lung retention of the aerosol. Furthermore, engineering the rate of size increase can be used to target deposition within specific regions of the lung. Factors influencing the amount and rate of size increase with the ECG approach include the degree of supersaturation, temperature, particle or droplet hygroscopicity, initial size, and aerosol number concentration.

Hygroscopic growth of aerosols in the respiratory tract at subsaturated relative humidity (RH) values has been widely reported.[11,12,48] In contrast, aerosol growth in supersaturated respiratory environments has been considered less frequently. Ferron et al.[10] observed that supersaturated conditions should occur in the nasal cavity during the inhalation of cool saturated air using a 1-D heat and mass transport model. Zhang et al.[61] developed a 3-D computational fluid dynamics (CFD) model of heat and mass transfer in the upper airways through approximately the fourth respiratory generation and reported supersaturated conditions for the inhalation of cool air with a RH of 80%. Both Ferron et al.[10] and Zhang et al.[61] observed significant aerosol growth in the region of supersaturation. However, aerosol evaporation was reported once RH values returned to wall conditions. In contrast, Longest and Xi[34] reported supersaturated air-phase conditions could exist over a large portion of the upper airways during the inhalation of warm saturated air a few degrees above body temperature. It was found that submicrometer aerosols in this environment exhibited significant size increase. Evaporation of the aerosol was not observed. However, the model of Longest and Xi[34] did not extend beyond the sixth respiratory generation.

Recent studies have demonstrated the effectiveness of pharmaceutical aerosol delivery to the lungs using ECG in a simple tubular system and a more advanced mouth-throat (MT) and tracheobronchial (TB) model.[17,29,38] Longest et al.[38] considered submicrometer aerosol growth in a simple tubular system designed to provide an aerosol residence time consistent with the time required to reach the main carina, i.e., approximately 0.2 s. Experimental measurements of droplet sizes indicated growth from initial mass median aerodynamic diameters (MMAD) in the range of 150–900 nm to 2–3 μm at number concentrations consistent with pharmaceutical aerosols. A corresponding numerical model illustrated the potential for continued growth over longer residence times and a significant increase in growth rate for minor increases in supersaturation levels. Longest and Hindle[29] developed a CFD model of pharmaceutical aerosol hygroscopic growth and validated the model with

comparisons to experimental data. CFD predictions of ECG in the tubular system indicated that size increase occurred over the length of the geometry and that two-way coupling was significant for dry wall conditions, in which the number concentration limited the rate of growth. Good agreement was observed between the CFD predictions and experimental growth results; however, aerosol deposition was not considered in the simple tubular geometry.

Hindle and Longest[17] evaluated ECG aerosol delivery in a realistic model of the MT and upper TB region extending to the fifth respiratory bifurcation (B5) down an individual path. Experimental results indicated that MT drug loss was minimal (~1%) and that TB deposition increased with ECG conditions, which implies significant aerosol growth. Specifically, ECG conditions were observed to increase deposition in branches B3–B5 by an order of magnitude compared to a control case without growth (~2% with ECG vs. 0.3% with control). The numerical predictions closely matched the experimental results of deposited drug within individual sections of the model and indicated a size increase of the initially submicrometer aerosol to 2–4 μm at the fifth respiratory bifurcation. As a result of this and previous studies, it can be concluded that ECG is an effective strategy for significantly reducing MT aerosol deposition and increasing droplet size to a target range of 2–4 μm, which is expected to produce nearly complete lung retention. However, it is not clear how far supersaturated conditions penetrate into the lungs during ECG delivery. It may be possible for some droplet evaporation to occur once the water vapor equilibrates with the wall conditions. Finally, the deposition profile of aerosols delivered under ECG conditions needs to be characterized throughout the TB airways to ensure lung retention of the aerosol. To address these issues, a model of ECG delivery within the medium and small TB airways is needed.

A number of recent papers have reported aerosol transport and deposition in realistic models of the upper TB airways usually extending to approximately the fourth through the ninth generations.[25,39,56] Gemic et al.[14] developed a CFD model of airflow in all generations of the TB region. However, the reported number of grid cells was likely not sufficient when compared to the grid convergence studies of Longest and Vinchurkar.[31] In a series of papers, Kleinstreuer et al. have developed a CFD model of aerosol transport and deposition throughout the TB region.[22,63] This model is based on repeating scaled triple bifurcation units in series and in parallel to characterize airflow and deposition in all 16 generations of an idealized TB tree. This approach is effective in evaluating deposition efficiency within individual branches. Lin et al.[27] reported a coupled 3-D and 1-D lung transport model that can mimic the entire TB region on a patient specific basis. In comparison with these recent studies, Koblinger and Hofmann[23] introduced the idea of a Monte Carlo lung simulation approach in which paths down the airway tree are generated at random and used for 1-D algebraic predictions of lung deposition. Deposition within these "individual paths" is used to build a representation of deposition within the lung. Application of this individual path approach to quantify deposition in the TB region has not previously been reported for a CFD model.

The objective of this study is to evaluate the ECG delivery of respiratory aerosols in an individual path model extending from the MT to the end of the TB region. Initially monodisperse aerosol sizes of 560 and 900 nm will be delivered, consistent with previous experimental studies of ECG.[38] Aerosol size change and deposition will be assessed for the inhalation of control subsaturated air and ECG conditions with saturated air and temperatures of 39 and 42 °C. A previously validated CFD model of aerosol transport and deposition during ECG delivery in the respiratory airways will be applied. The geometry consists of a previously developed MT, a model of the TB airway extending to bifurcation B3, and a subsequent individual path model entering the right lower lobe of the lung. Results

of this study will be used to assess (i) temperature and RH conditions in the medium and small TB airways during ECG delivery, (ii) the potential for aerosol evaporation during ECG, (iii) the potential for deposition in the medium and small TB airways for control and ECG aerosols, and (iv) targeted aerosol deposition based on the initial ECG conditions.

METHODS

MT-TB Geometry

The geometry considered in this study (Fig. 1) consists of the MT region, the upper TB airways extending from the trachea to the third respiratory bifurcation (B3), and an individual path model of the medium and small TB airways extending to the terminal bronchioles (B15). The trachea and the initial part of the main bronchi constitute bifurcation B1. The MT geometry is the elliptical model proposed by Xi and Longest[54] and contains the oral cavity, pharynx, and larynx. This geometry is based on the oral airway cast reported by Cheng *et al.*[8] and in-house CT data of the pharynx and larynx.

The upper TB airways are represented with an approximate model extending through the third bifurcation. This asymmetrical model was based on the anatomical cast dimensions reported by Yeh and Schum[58] and scaled to a functional residual capacity (FRC) of 3.5 L, which is consistent with an adult male.[19] The individual bifurcation units were generated using the physiologically realistic bifurcation (PRB) parameters reported by Heistracher and Hofmann.[16] However, modifications to the equations reported by Heistracher and Hofmann[16] were required to generate smooth asymmetrical bifurcations. Surface properties of the bifurcations such as carinal ridge and branch radii of curvatures were taken from the measurement studies of Horsfield *et al.*[18] and Hammersley and Olson.[15] These bifurcation units were rotated out of plane to approximate the gravity angles specified by Yeh and Schum.[58] In the TB model, B2 of the left lung feeds the left upper and left lower lobes. In the right lung, B2 feeds the right upper lobe directly, whereas the lower third bifurcation feeds the right middle and right lower lobes.

The upper TB model applied in this study is intended to be a general representation of the airways that includes asymmetry, out of plane rotation, and previously documented branch diameters, lengths, and bifurcation angles. The effects of cartilaginous rings on deposition have been previously reported[40,47,60] and are not included in this study. Some additional differences between the current model and previous cast and scanned TB geometries[26,46,56] are also observed. For example, the right main bronchus is longer than in the previous cast-based geometry of Xi *et al.*,[56] due to the use of mathematically generated PRB units. Still, the asymmetrical model is considered to be sufficiently accurate to characterize aerosol growth and deposition in the upper airways, which will be verified with comparisons to the upper TB deposition data of Zhou and Cheng.[64]

Beyond the third bifurcation, an individual path model was considered extending down the right lower lobe. Use of the individual path model based on PRB units allows for the application of a hexahedral mesh, which improves solution accuracy, and an adequate number of computational cells to fully resolve the flow domain.[52] Bifurcations within the model were constructed as PRB units with the airway dimensions reported by Yeh and Schum,[58] again scaled to a FRC of 3.5 L. Based on available data, the bifurcations in the individual path model section (B4-B15) were symmetric and include a symmetric outflow assumption at each bifurcation level. At each bifurcation, continuation of the left or right branch was selected at random. However, if the selection led out of the general region of the right lower lobe, the other branch was selected. Consecutive branches were rotated at 90° to approximate physiological conditions.[45] This individual path model is not intended to exactly mimic a specific connection of bronchi as with a patient specific model. Instead, it is

intended to provide an effective 3-D representation of transport and deposition in the medium and small TB airways. Branch 15 was assumed to end with the terminal bronchioles, based on existing anatomical data.[58]

Boundary and Delivery Conditions

Separate streams of aerosol and humidified air are delivered to the mouth inlet for both control and ECG growth conditions. As shown in Fig. 1, the aerosol stream is delivered through an inner cross-sectional circle whereas the humidified air is delivered through an outer ring at the mouth inlet. To maintain separation of these streams until mixing in the MT occurs, Hindle and Longest[17] developed and presented a dual flow mouthpiece. As reported by Hindle and Longest,[17] the inlet areas of the aerosol and humidity streams are balanced to maintain a constant velocity. The total inlet flow rate considered in this study is approximately 30 L/min under steady state conditions.

The airway walls were assumed to be at body temperature and lined with isotonic mucus. As a result, the RH of the airway wall was set at 99.5%. Previous studies have reported variable wall temperatures from the mouth to core body temperature downstream. However, correlations describing this change are based on the inhalation of ambient environmental conditions. During ECG delivery, which is via a nebulizer and requires multiple inhalations, [17] it is expected that the inhalation of warm air will significantly decrease any airway wall temperature gradients. The walls of the airway model are assumed fixed and rigid.

Outflow conditions from the upper TB model into each lung lobe were based on the estimates of Horsfield et al.[18] Beyond the lobar bronchi, symmetric outflow conditions were assumed at each bifurcation level (B4- B15). This assumption is not expected to largely influence the growth and regional deposition characteristics of interest in this study.

Aerosol and humidified air inlet conditions are shown in Table 1 for the delivery of 560 and 900 nm droplets. Both control and ECG delivery cases were considered. For the control scenarios, the aerosol was delivered with ambient air and assumed to be a non-evaporating particle (Case 1) or a droplet experiencing either evaporation or condensation (Case 2). ECG conditions were evaluated as the remaining two cases. Under these conditions, the aerosol and humidified air were delivered at either 39 °C (Case 3) or 42 °C (Case 4). Increasing the aerosol and humidity stream temperatures allows for more water vapor mass to be delivered to the airways, which is expected to increase the final aerosol size and alter the deposition profile. Albuterol sulfate (AS) was considered as a model drug in the aerosol. The mass fractions of drug in the initial 560 and 900 nm droplets were assumed to be 31% and 49%, respectively, based on a previous experimental study in which these aerosols were formed using a small particle aerosol generator.[38] At these mass fractions, the hygroscopic effects of AS are expected to enhance size increase initially for RH values below 100%. However, hygroscopic effects are expected to significantly diminish once the aerosol increases in size above approximately 1 μ.[38]

Deposition Factors

Deposition within regions of the respiratory tract can be reported as either a fraction or efficiency. The deposition fraction (DF) for the ith region is calculated as

$$DF_i = \frac{\text{number of particles depositing in region } i}{\text{number of particles entering the mouth}}$$

(1)

In contrast, the corresponding deposition efficiency (DE) for region i is calculated as

$$DE_i = \frac{\text{number of particles depositing in region } i}{\text{number of particles entering region } i} \qquad (2)$$

To determine a total deposition fraction, DF_i values in individual regions can be directly summed. Deposition efficiency values are an effective method to report the characteristics of an individual section of the respiratory tract without the influence of upstream aerosol losses. In this study, DE values are calculated for each bifurcation. Sectional DE values are then computed by combining the individual bifurcation values.[19] For example, the DE in region B4 to B7 is calculated as

$$DE_{B4-B7} = 1 - (1 - DE_{B4})(1 - DE_{B5}) \times (1 - DE_{B6})(1 - DE_{B7}) \qquad (3)$$

The total DF for the entire MT-TB network is then calculated as

$$DE_{MT-TB} = 1 - \prod_{i=1}^{I}(1 - DE_i) \qquad (4)$$

which includes all regions ($i = 1$ to I) from the MT to B15. It is noted that the total DE of the model is equal to the total DF.

CFD Simulations

A CFD model was implemented that can accurately simulate local temperature and humidity fields, together with droplet trajectories, size change, and deposition within the MT-TB model during ECG aerosol delivery. To effectively address both laminar and turbulent flow conditions, a low Reynolds number (LRN) k-ω turbulence model was selected. This model has previously been well-tested, and found to provide good estimates of aerosol transport and deposition in upper airway geometries.[32,56] To evaluate the variable temperature and RH fields in the MT-TB model, interconnected relations governing the transport of heat and mass (water vapor) were also included. These governing equations were previously presented in detail by Longest and Xi[34] and Longest et al.[35]

To model droplet trajectories, growth, and deposition, a previously developed and tested combination of a commercial code (Fluent 6.3, ANSYS Inc.) and user functions was implemented. User routines were employed to better model near-wall conditions and to simulate aerosol condensation and evaporation in the complex three-dimensional temperature and humidity fields. Previous studies have shown that the isotropic turbulence approximation, which is assumed with the LRN k-ω model, can over predict aerosol deposition.[41] As a result, a user routine was employed to account for anisotropic near-wall turbulence, as described by Longest et al.[35] Other additions to the particle tracking model included (i) a correction to better predict the Brownian motion of submicrometer aerosols and (ii) improved near-wall interpolation of fluid velocities.[33]

A user routine was employed to model interconnected droplet temperature and size change resulting from condensation and evaporation. This droplet model accounts for the Kelvin effect, hygroscopicity arising from the dissolved drug, and the effect of droplet temperature on surface vapor pressure. In simulating aerosol evaporation and growth, the effect of the droplets on the continuous phase was typically neglected, resulting in a one-way coupled approach. One-way coupled simulations are expected to be accurate in this study due to the presence of wetted walls. However, to assess the validity of this assumption, the effect of the

discrete aerosol phase on the continuous heat and water vapor fields was also included in some simulations, which is referred to as two-way coupling. An experimentally measured concentration of 2.8×10^5 particles/cm^3 for the 900 nm aerosol (after mixing with the humidity stream) was employed to assess the two-way coupling effects.

In performing the CFD simulations, previously established best-practices were implemented to provide a high quality solution. All transport equations were discretized to be at least second order accurate. The computational mesh was constructed in Gambit 2.4 (ANSYS, Inc.) and consisted entirely of hexahedral elements (Fig. 2), which provide a higher quality solution than commonly employed tetrahedral grids.[52] Convergence of the flow field solution was assumed when the global mass residual had been reduced from its original value by five orders of magnitude and when the residual reduction rates for both mass and momentum were sufficiently small. To improve accuracy and to better resolve the significant change in flow scales during deposition, all calculations were performed in double precision. For the MT-TB model, grid convergent results were found to occur with meshes consisting of approximately 2.4 million control volumes. In order to produce convergent deposition results, 120,000 initial droplets were released for each of the two aerosol sizes considered. MMAD values after growth were calculated based on the midpoint diameters of a standard Andersen cascade impactor.[53] Doubling the number of droplets considered had a negligible impact on both total and sectional deposition results.

Model Validation

The CFD model employed in this study has previously been extensively tested in comparison with experimental deposition results. For both constantsized particles and evaporating droplets, the CFD model was shown to accurately predict local and sectional deposition profiles in comparison with in vitro experiments.[28,32,37] Longest and Hindle[29] recently presented a CFD model of ECG aerosol delivery in detail. In this study, excellent agreement was found between experimental measurements of final particle size after condensational growth and CFD predictions. Hindle and Longest[17] compared *in vitro* results and numerical predictions of aerosol drug deposition in a MT–TB geometry extending to the fifth respiratory generation. Good agreement was found between the experimental and numerical predictions of deposition for both control and ECG conditions on a sectional basis and for the entire MT–TB geometry.

Comparison of Upper TB Deposition to Previous Studies

As discussed, some differences are observed between the upper TB model considered in this study and previously reported models. An advantage of the current model is the use of a standard well described bifurcation unit (the PRB) that can be reproduced by other researchers. Furthermore, the characteristic TB model considered can accommodate a hexahedral mesh. However, differences in deposition from potentially more realistic models may be a concern. To address this issue, deposition in the current upper TB model was compared to the experimental results of Zhou and Cheng[64] on a regional basis. Particles in the range of 0.93–30 lm were considered at an inhalation flow rate of 30 L/min. As shown in Fig. 3, deposition efficiencies in the trachea, first bifurcation, second bifurcation, and third bifurcation provide an excellent match to the experimental data. As a result, it is concluded that the current model is sufficiently detailed to capture regional deposition characteristics in the upper TB airways. Furthermore, this comparison provides an additional validation study indicating that our CFD model is accurate.

RESULTS

Continuous Field Variables

Contours of temperature are shown for the MT, upper TB airways, and selected medium and small TB airways in Fig. 4 for Cases 2 and 4. Temperature contours are presented as mid-plane slices within each of the airway regions shown. For Case 2 conditions, the initially cool 25 °C airstream is rapidly warmed by effective mixing in the MT and reaches approximately 30–34 °C in the trachea. Temperatures are generally above 34 °C in B4–B7 and near 37 °C in B12–B15. However, some areas below 36.5 °C are observed in the distal airway branches. For the inhalation of 42 °C saturated air (Case 4), rapid cooling is observed in the MT with temperatures in the range of 39–41 °C in the trachea. Elevated temperatures of approximately 38 °C are observed in B4–B7 and temperature is nearly uniform at 37 °C in the B12–B15 region.

Contours of RH for Cases 2 and 4, presented as midplane slices, are illustrated in Fig. 5. As expected, the cool subsaturated inlet conditions of Case 2 result in low RH values through a majority of the upper TB airways. Due to mass transfer from the wet walls, RH values of 95% and greater are observed in bifurcations B4–B7. In the distal bifurcations B12-B15, RH values are predominately equal to the wall value of 99.5%. However, contour levels below walls conditions are also observed even in the most distal airways considered. For Case 4 inlet conditions, rapid cooling of the saturated airstream results in a rapid progression to supersaturation, with values as high as 103% observed in the pharynx. RH values remain in the range of 101–103% through a majority of the upper TB geometry and bifurcations B4–B7. In B12–B15, RH values are near wall conditions, but remain in the range of 99.5–101%.

Aerosol Transport and Growth

Trajectories of initially monodisperse 900 nm droplets in the full MT–TB geometry are illustrated in Fig. 6 for Cases 2–4. Considering Case 2, rapid droplet evaporation occurs in the oral cavity until only a solid drug particle remains. As RH increases due to the warm and wet walls, some hygroscopic growth of the aerosol is observed with B15 trajectories in the range of 0.9–1.0 μm. For ECG delivery (Cases 3 and 4), rapid aerosol growth is observed throughout the MT and first bifurcation. In the medium and small TB branches, growth slows due to reduced RH values and a decreased hygroscopic effect associated with higher droplet mass fractions of water. However, slower droplet velocities in the more distal airways allow more time for growth to occur. The net result is observed to be continued growth without visible evaporation throughout the airways. For Cases 3 and 4, individual trajectories passing through bifurcation B15 are found to have increased in size from 900 nm to ranges of 2 to >2.5 μm and 2.5 to >3 μm, respectively.

Droplet size distributions sampled at specific cross-sectional locations in the model are presented in Fig. 7 in terms of mass fraction per micrometer of sampling bin size. MMAD values are also presented for each aerosol size distribution. Considering Case 2, MMAD values change little from the initial sizes of 560 and 900 nm. However, mixed evaporation and hygroscopic growth result in a spreading of the size distribution from the initial monodisperse condition. In contrast with Case 2, ECG conditions result in a definite shift in the distribution profile to larger sizes. Considering Case 3 and initial sizes of 560 and 900 nm, both the MMAD and size distribution indicate significant and successive growth at the tracheal inlet and B5 outlet. However, some decrease in MMAD size is observed between the B5 outlet and B15 outlet for the 560 (~0.4 μm reduction) and 900 nm (~0.2 μm reduction) aerosols. This decrease in MMAD may arise from (i) deposition of the larger particles and (ii) minor evaporation as RH approaches 99.5%. Considering that only a small size decrease is observed for the 900 nm aerosol under Case 3 conditions, the decrease of the

560 nm aerosol is likely due to minor evaporation arising from a lower drug concentration in the droplet and a reduced hygroscopic effect. Under Case 4 delivery conditions, size decreases between the B5 and B15 outlets of approximately 0.2 μm are observed for both aerosol sizes. Size distribution profiles indicate that 20–40% of the aerosol mass is associated with droplets of 4 μm and above. Furthermore, RH values shown in Fig. 5 were generally above 100% for Case 4 delivery conditions. As a result, this minor decrease in aerosol size may be primarily due to the deposition of larger droplets in the bifurcating airways.

MMADs of the polydisperse aerosol entering each bifurcation (B1–B15) are presented in Fig. 8 for the various delivery conditions. For Case 2, results indicate sudden evaporation followed by very slow growth, as expected. Considering the ECG conditions, rapid growth is observed from the mouth to the tracheal (B1) inlet. It is noted that the reported MMADs are calculated over all droplets entering each bifurcation, i.e., as they cross the inlet plane. However, details of growth for the aerosol ensemble are not resolved within each model segment due to the number of droplets considered. In the figure, significant growth is observed to occur through approximately B3. Thereafter, minor growth is observed through approximately B8, and some size decrease occurs between B8 and B15. As described above, this size decrease is generally in the range of 0.2–0.4 μm and likely arises from both deposition and minor evaporation; however, deposition appears to be the primary cause.

To evaluate the validity of the one-way coupled assumption, two-way coupled simulations were also considered. In two-way coupling, heat and mass transfer from the droplets are accounted for as source terms in the continuous phase equations and influence subsequent droplet size change. The 900 nm aerosol was considered under Case 3 and 4 conditions, where the effects of two-way coupling are expected to be the strongest.[38] An aerosol concentration of 2.8×10^5 particles/cm^3 was considered, based on the experimental study of Longest *et al.*,[38] in which the 900 nm aerosol was formed. In general, two-way coupling is expected to slow both size decrease and increase as changes in air phase RH damp evaporation and condensation. However, the simulation results indicate that two-way coupling has a minimum effect on aerosol size change, likely because of the wet-wall boundary conditions. Specifically, relative percent differences were calculated as | $MMAD_{one-way}$ − $MMAD_{two-way}$|/$MMAD_{two-way}$ × 100. Percent differences in MMADs for aerosols entering the trachea and exiting B5 were less than approximately 10%. At B15, relative percent differences were less than 5%.

Aerosol Deposition

Deposition locations of individual droplets are illustrated for the 900 nm aerosol with Case 2 and 4 delivery conditions in Fig. 9. The droplets are colored based on their size at the time of deposition. Deposition efficiencies were calculated for each bifurcation and then combined (e.g., Eq. (3)) to represent the total deposition efficiencies for the sections reported along the individual path. Considering Case 2, very little deposition is observed with a maximum of only 7.1% in the airways B8–B15. For ECG delivery conditions, the MT deposition efficiency remains very small (~1%) as observed by Hindle and Longest.[17] In contrast with this low MT value, deposition efficiencies in B4–B7 and B8–B15 are increased by an order of magnitude compared with the evaporating control case (Case 2). Furthermore, deposited particles beyond B4 are predominately 3 μm and above, which provides evidence that the observed minor reduction in MMAD is due to the loss of the larger aerosols in the polydisperse size distribution.

A complete description of deposition efficiencies for each case considered is presented in Fig. 10 and Table 2. Deposition efficiencies are again calculated as the combination of the values determined for each bifurcation. For all cases, MT and upper TB deposition remained

extremely low (approximately <2%). Deposition in the more distal airways is then observed to increase by an order of magnitude for the ECG conditions (Cases 3 and 4) vs. the controls (Cases 1 and 2). For both initial sizes, Case 4 conditions approximately double deposition in B4–B7 and increase deposition in B8–B15 by a relative difference of approximately 25% compared with Case 3. Considering the ECG growth cases, minor differences in regional deposition efficiencies are observed for the initial 560 nm aerosol vs. the 900 nm aerosol. As a result, it appears that overall deposition is more influenced by inlet conditions than initial aerosol size.

Predicted total DEs of the TB airways are compared with the *in vivo*-based correlations of Stahlhofen *et al*.[50] and Chan and Lippmann[6] in Table 3. To calculate the total DE of the TB region from the CFD predictions, the deposition efficiencies of each bifurcation were combined using an expression similar to Eq. (3) from B1 to B15. The major assumption here is that the DEs of each bifurcation in the right lower lobe single path are representative of conditions in the other four lung lobes. For comparison, the TB correlations based on *in vivo* deposition data from Stahlhofen *et al*.[50] (Eq. 15) and Chan and Lippmann[6] (Eq. 3) were employed. The single characteristic aerosol size required in these correlations was assumed to be the calculated MMAD exiting B5, as shown in Table 3. The tracheal inlet flow rate of 30 L/min used in the CFD simulation was approximated in the correlations as an inhalation flow rate of 500 cm^3/s with an inhalation volume of 1500 cm^3 to represent deep inspiration, which is characteristic of pharmaceutical aerosol delivery. As shown in Table 3, the predicted DEs from this study are in general agreement with the *in vivo* data, but the CFD predictions are somewhat higher. Considering the *in vivo* variability reported by Stahlhofen *et al*.,[50] it is observed that the CFD predictions are well within the range of the experimental data. The CFD predictions are likely higher than the mean experimental data because of the use of a single lobe and single path model to represent the remainder of the TB airways, a larger CFD lung volume than in the experiments (3.5 vs. ~3.0 L), and the use of a single droplet diameter to account for the deposition of a polydisperse aerosol that is increasing in size.

To approximate whole lung retention of the aerosol, the MT–TB deposition fractions predicted with Eq. (4) are reported in Table 4. These values are combined with the alveolar deposition efficiency correlation of Stahlhofen *et al*.[50] to provide estimates of total lung deposition (DF_{total}). Again, an inhalation rate of 500 cm^3/s was employed along with a volume of 1500 cm^3. As observed from Table 4, total lung deposition fractions for the ECG conditions are 90% and above, except for Case 3 and the 560 nm aerosol, where the DF_{total} is 83%. These whole lung deposition values could be increased further with the inclusion of a breath pause. In contrast, for both controls (Cases 1 and 2), the total lung deposition fraction was between approximately 23–38%.

DISCUSSION

In this study, the concept of ECG applied to respiratory drug delivery was tested in a representative airway model extending from the oral cavity to the end of the TB airways. Droplet transport, size change, and deposition were simulated using a previously well-tested and experimentally validated CFD model. Simulations were conducted in a previously developed MT geometry and a new characteristic model of the upper TB airways based on mathematically characterized PRB units. For the first time, aerosol transport and deposition throughout the TB region was approximated using an individual path model and CFD simulations. Results indicate that both control and ECG delivery conditions produce very little deposition and aerosol loss in the MT and upper TB airways. With ECG delivery, significant size increases of the initially submicrometer aerosols were observed to occur, resulting in MMADs of 2–3 μm in the medium and small TB airways. This increase in

aerosol size was shown to produce an order of magnitude increase in drug deposition in the TB airways, with TB deposition efficiencies of approximately 32–46% for ECG conditions. Estimates of downstream pulmonary deposition indicted near full lung retention of the aerosols during ECG delivery.

As previously demonstrated by Hindle and Longest,[17] delivering pharmaceutical aerosols using the ECG approach resulted in very low MT deposition (~1%). In contrast, MT depositional losses are currently reported as ~60% for a typical MDI with a HFA propellant, [9] ~70% for a typical DPI,[62] and 30–40% for state-of-the-art breath-actuated nebulizers.[43,44] For the same MT and similar upper TB geometry as considered in this study, Hindle and Longest[17] reported experimental values of drug deposition using a Proventil HFA MDI. The mean (and standard deviation) AS deposition in the MT–TB model was found to be 49.7 (7.2)% of the dose. The majority of the dose from the MDI was deposited in the MT region (46.0%), with only 3.6% deposited in the B1–B5 airways. Minor differences between this study and that of Hindle and Longest[17] include the use of an initially monodisperse aerosol and an upper TB model that is complete through B3 in the current study. Equivalent aerosol and humidity inlet temperatures are also employed for ECG conditions in the current study, which were only considered for one case in Hindle and Longest.[17] As a result, MT and upper TB deposition values are slightly different than previously reported. However, the primary motivation behind the current study was to investigate conditions throughout an individual path model of the entire TB region.

Prior to this study, airway conditions and aerosol behavior in the medium and small TB bifurcations was unknown for ECG delivery. Previous results of aerosol size change during the inhalation of cool saturated air in the upper airways indicated that aerosol size increase may be temporary and some evaporation may occur.[10,61] However, results of this study indicate that with the inhalation of warm saturated air, several degrees above body temperature, supersaturated conditions extend well into the respiratory tract. This increased region of supersaturation likely occurs due to the larger mass of water vapor that enters the airways with the inhalation of warm vs. cool saturated air. As a result of extensive supersaturation in the flow field, aerosol growth was observed to occur throughout a majority of the TB airways without visible evaporation of individual trajectories under ECG conditions. Minor decreases in the aerosol MMAD were observed beginning with B8 (Fig. 8). However, this decrease in MMAD can be largely explained as resulting from the higher deposition fraction of the larger droplets in the medium and small TB bifurcations (Fig. 9). With ECG, deposition within the TB airways beginning with B4 was increased by an order of magnitude compared to the evaporating control case resulting in single path deposition efficiencies of 32–46%. Aerosols exiting B15 had MMADs ranging from 2.00 to 2.95 μm. As a result of these observations, it is concluded that the advantages of ECG delivery are maintained throughout the TB region and that negligible evaporation of individual droplets occurs. Furthermore, estimates indicate that alveolar deposition will result in near full lung retention of the aerosol (Table 4). Based on the aerosol behavior observed in the medium and small TB airways, only negligible evaporation is expected in the alveolar region.

For the prescribed inhalation flow conditions ($Q = 500$ cm^3/s and $V_T = 1500$ cm^3), application of the Stahlhofen et al.[50] equation for alveolar deposition in combination with the TB deposition values predicted in this study indicated near full lung retention of the aerosol with ECG delivery. The alveolar estimates are based on the aerosol size exiting B15, which is approximately 3 μm for ECG conditions. It is noted that full lung retention of an aerosol is significantly influenced by both particle size and inhalation parameters. *In vivo* studies of the full lung deposition of monodisperse stable 3 μm particles indicate that retention may be less than 100% for different breathing parameters. For example, the review article of Kim[21] shows that the *in vivo* total lung deposition fraction of a 3 μm aerosol with

$Q = 500$ cm^3/s and $V_T = 1000$ cm^3 is approximately 60% based on a bolus delivery technique. One factor that may contribute to the predicted high lung deposition values compared with previous *in vivo* studies is that the approximate aerosol size of 3 μm is based on droplets which have not deposited and exit B15. It is difficult to determine a representative droplet size for predicting full lung deposition with ECG due to the combination of both active growth and deposition in the airways. Figure 9 clearly shows that the majority of deposited particles are greater than 3 μm and further analysis of the data indicates a number of deposited 4 μm particles. Table 3 also shows that the CFD predicted values for TB deposition are representative of, but greater than, the corresponding correlation-based values using an average static inlet diameter. Therefore, 3 μm may be a small approximate static size for comparing the predictions of the current study with previously reported whole lung deposition data. Further investigation is needed to better predict deposition in the alveolar region and to approximate the total lung doses delivered with ECG. However, the CFD predictions of TB deposition presented in this study are expected to be accurate based on the extensive validations that have previously been performed in terms of both aerosol size increase and deposition.[17,29]

In addition to significantly reducing MT deposition and enabling full lung retention, results also illustrate the ability of ECG to target deposition within regions of the TB airways. Specifically, increasing the ECG delivery temperature from 37 to 39 °C approximately doubled the amount of drug mass deposited in region B4–B7 (e.g., 4.7–9.2%). This increase was observed for both aerosol sizes. Increasing both the delivery temperature and initial size increased deposition in B8–B15 by a factor of 1.25 (e.g., 28.6–37.0%). In general, the initial size of the aerosol (560 vs. 900 nm) had a minor influence on the final size and deposition fraction. As observed by Longest *et al.*,[38] surrounding temperature and RH conditions and not initial size generally control the final aerosol size achieved with ECG delivery. However, the initial size may become a more significant factor if hygroscopic effects are larger, for high number concentration aerosols, and if shorter times are available for growth as may occur with targeted upper airway delivery. The observed variations in TB deposition associated with ECG initial conditions may be reduced *in vivo* due to variations in patient anatomy and inhalation profiles. Furthermore, ECG does not provide a means to produce highly localized targeted deposition, as may potentially be achieved with magnetic aerosols.[57]

In this study, an individual path model was used for the first time to characterize flow field conditions and aerosol transport from the fourth bifurcation to the end of the TB region. As indicated above, this approach is not intended to fully resolve all pathways throughout the conducting airways. Instead, it serves as a representative model for assessing transport and deposition. In future analyses, it is proposed to use individual paths to stochastically characterize transport and deposition within the bifurcations of each lung lobe. Randomly generated individual path models can be simulated to create an ensemble of deposition efficiencies. Averages of these ensemble results can then be used to quantify transport conditions and deposition fractions (branch-averaged and highly localized) on a stochastic basis. However, a full characterization of the entire TB tree was not necessary to achieve the objective of this study. In this study, deposition efficiencies calculated from each branch of the individual path model were used to estimate total deposition in the TB region. The fact that these estimates were in general agreement with existing correlations for TB deposition *in vivo* provided evidence that the individual path model approach is reasonable and also supports the accuracy of the CFD predictions.

The predicted MT deposition of approximately 1–2% may initially appear low considering that the typical aerosol size entering the trachea is 2 μm with ECG conditions. Furthermore, the elliptical MT model is known to be a representation of a more realistic geometry.[54] The

previous study of Longest *et al.*[36] showed that 2 μm particles at a steady flow rate of 30 L/min resulted in a MT deposition of approximately 5%. Xi and Longest[54] reported that the deposition of a 2 μm aerosol in the MT model at 30 L/min was approximately 10%. Several factors contributed to the observed reduction in MT deposition in this study. First, droplet growth occurs continuously, so the actual deposition is expected to be smaller than would occur for the final aerosol size at the MT outlet. Second, the dual flow mouthpiece centralized the aerosol and surrounded it with a layer of clean air. The previous study of Longest and Oldham[30] showed that reducing the aerosol inlet cross-sectional area could significantly reduce aerosol deposition. The deposition results of Xi and Longest[54] are likely high for particles in the 1–2 μm size range, because of the use of the k–ω turbulence model without an anisotropic correction, as employed in the current study. However, the results of Xi and Longest[54] did show very little difference in the MT total deposition values between a more realistic geometry and the current elliptical model at 30 L/min, which provides a justification for the use of the elliptical model. The low MT deposition values of the current study are in good agreement with the experimental upper airway results of Hindle and Longest,[17] which further supports the validity of the current simulations. However, some differences between the *in vitro* data and current results likely arise due to the factors described above, such as the implementation of an initially monodisperse aerosol distribution with the CFD model of this study.

Limitations of the current study are associated with the geometry employed, simulation conditions, and numerical model. As previously discussed, the MT and upper TB models implemented some simplifications to facilitate a mathematically described geometry and allow for the use of more accurate hexahedral meshes.[52] Furthermore, wall motion of the airways, particularly in the range of B15, may influence aerosol deposition. The assumed rotation angle of 90° for successive bifurcations may also be an overestimation of physiological conditions. The current model assumed steady state flow, which may impact the transport and deposition of some near-wall particles in the distal branches. The lobar ventilation rates were based on the volume estimates of Horsfield *et al.*[18] More accurate representations may be available from numerical models[1,2] or for supine individual patients.[59] Higher accuracy representations of the turbulent laryngeal jet can be computed with more time intensive models, such as direct numerical simulation and large eddy simulation.[26,42] However, our previous results indicate good agreement between the LRN k–ω approximation with near-wall corrections and experimental predictions of growth and deposition.

In conclusion, ECG delivery resulted in supersaturated RH fields throughout large portions of the TB airways. Initial submicrometer aerosols were observed to increase in size to a target range of 2–4 μm and evaporation of individual droplets was not evident. As a result, ECG provides an effective method to virtually eliminate MT depositional losses, and the associated intersubject variability, while providing for high TB deposition and near full lung retention of the aerosol. Targeting drug deposition within specific lung regions was also demonstrated. Future studies are needed to consider the effects of unsteady flow, drug concentrations in the droplets, additional individual path models for full TB characterization, and deposition in the alveolar region with moving boundaries.

Acknowledgments

REFERENCES

1. Asgharian B, Price OT. Airflow distribution in the human lung and its influence on particle deposition. Inhal. Toxicol 2006;18:795–801. [PubMed: 16774869]

2. Asgharian B, Price OT, Hofmann W. Prediction of particle deposition in the human lung using realistic models of lung ventilation. Aerosol Sci 2006;37:1209–1221.

3. Azarmi S, Roa WH, Lobenberg R. Targeted delivery of nanoparticles for the treatment of lung diseases. Adv. Drug Deliv. Rev 2008;60:863–875. [PubMed: 18308418]

4. Borgstrom L, Olsson B, Thorsson L. Degree of throat deposition can explain the variability in lung deposition of inhaled drugs. J. Aerosol Med 2006;19:473–483. [PubMed: 17196076]

5. Byron PR. Drug delivery devices: issues in drug development. Proc. Am. Thorac. Soc 2004;1:321–328. [PubMed: 16113453]

6. Chan TL, Lippmann M. Experimental measurements and empirical modeling of the regional deposition of inhaled particles in humans. Am. Ind. Hyg. Assoc. J 1980;41:399–409. [PubMed: 7395753]

7. Cheng YS. Aerosol deposition in the extrathoracic region. Aerosol Sci. Technol 2003;37:659–671. [PubMed: 19011693]

8. Cheng KH, Cheng YS, Yeh HC, Swift DL. Measurements of airway dimensions and calculation of mass transfer characteristics of the human oral passage. J. Biomech. Eng 1997;119:476–482. [PubMed: 9407288]

9. Cheng YS, Fu CS, Yazzie D, Zhou Y. Respiratory deposition patterns of salbutamol pMDI with CFC and HFA-134a formulations in a human airway replica. J. Aerosol Med 2001;14(2):255–266. [PubMed: 11681657]

10. Ferron GA, Haider B, Kreyling WG. Conditions for measuring supersaturation in the human lung using aerosols. J. Aerosol Sci 1984;15:211–215.

11. Ferron GA, Oberdorster G, Hennenberg R. Estimation of the deposition of aerosolised drugs in the human respiratory tract due to hygroscopic growth. J. Aerosol Med 1989;2:271.

12. Finlay WH. Estimating the type of hygroscopic behavior exhibited by aqueous droplets. J. Aerosol Med 1998;11(4):221–229. [PubMed: 10346665]

13. Finlay WH, Martin AR. Recent advances in predictive understanding of respiratory tract deposition. J. Aerosol Med. Pulm. Drug Deliv 2008;21(2):189–205. [PubMed: 18518795]

14. Gemci T, Ponyavin V, Chen Y, Chen H, Collins R. Computational model of airflow in upper 17 generations of human respiratory tract. J. Biomech 2008;41(9):2047–2054. [PubMed: 18501360]

15. Hammersley JR, Olson DE. Physical models of the smaller pulmonary airways. J. Appl. Physiol 1992;72:2402–2414. [PubMed: 1629097]

16. Heistracher T, Hofmann W. Physiologically realistic models of bronchial airway bifurcations. J. Aerosol Sci 1995;26(3):497–509.

17. Hindle M, Longest PW. Evaluation of enhanced condensational growth (ECG) for controlled respiratory drug delivery in a mouth-throat and upper tracheobronchial model. Pharm. Res 2010;27:1800–1811. [PubMed: 20454837]

18. Horsfield K, Dart G, Olson DE, Cumming G. Models of the human bronchial tree. J. Appl. Physiol 1971;31:207–217. [PubMed: 5558242]

19. ICRP. Human Respiratory Tract Model for Radiological Protection. Elsevier Science Ltd.; New York: 1994.

20. Jaques PA, Kim CS. Measurement of total lung deposition of inhaled ultrafine particles in healthy men and women. Inhal. Toxicol 2000;12(8):715–731. [PubMed: 10880153]

21. Kim CS. Deposition of aerosol particles in human lungs: in vivo measurement and modeling. Biomarkers 2009;14(S1):54–58. [PubMed: 19604060]

22. Kleinstreuer C, Zhang Z. An adjustable triple-bifurcation unit model for air-particle flow simulations in human tracheobronchial airways. J. Biomech. Eng 2009;131:021007. [PubMed: 19102566]

23. Koblinger L, Hofmann W. Monte Carlo modeling of aerosol deposition in human lungs. Part I: simulation of particle transport in a stochastic lung structure. J. Aerosol Sci 1990;21(5):661–674.

24. Lai SK, Wang Y-Y, Hanes J. Mucus-penetrating nanoparticles for drug and gene delivery to mucosal tissues. Adv. Drug Deliv. Rev 2009;61:158–171. [PubMed: 19133304]

25. Li Z, Kleinstreuer C, Zhang Z. Particle deposition in the human tracheobronchial airways due to transient inspiratory flow patterns. Aerosol Sci 2007;38:625–644.

26. Lin C-L, Tawhai MH, McLennan G, Hoffman EA. Characteristics of the turbulent laryngeal jet and its effect on airflow in the human intra-thoracic airways. Respir. Physiol. Neurobiol 2007;157:295–309. [PubMed: 17360247]

27. Lin C-L, Tawhai MH, McLennan G, Hoffman EA. Multiscale simulation of gas flow in subject-specific models of the human lung. IEEE Eng. Med. Biol 2009;28:25–33.

28. Longest PW, Hindle M. Evaluation of the Respimat Soft Mist inhaler using a concurrent CFD and in vitro approach. J. Aerosol Med. Pulm. Drug Deliv 2009;22(2):99–112. [PubMed: 18956950]

29. Longest PW, Hindle M. CFD simulations of enhanced condensational growth (ECG) applied to respiratory drug delivery with comparisons to in vitro data. J. Aerosol Sci 2010;41:805–820. [PubMed: 20835406]

30. Longest PW, Oldham MJ. Mutual enhancements of CFD modeling and experimental data: a case study of one micrometer particle deposition in a branching airway model. Inhal. Toxicol 2006;18(10):761–772. [PubMed: 16774865]

31. Longest PW, Vinchurkar S. Effects of mesh style and grid convergence on particle deposition in bifurcating airway models with comparisons to experimental data. Med. Eng. Phys 2007;29(3): 350–366. [PubMed: 16814588]

32. Longest PW, Vinchurkar S. Validating CFD predictions of respiratory aerosol deposition: effects of upstream transition and turbulence. J. Biomech 2007;40:305–316. [PubMed: 16533511]

33. Longest PW, Xi J. Effectiveness of direct Lagrangian tracking models for simulating nanoparticle deposition in the upper airways. Aerosol Sci. Technol 2007;41:380–397.

34. Longest PW, Xi J. Condensational growth may contribute to the enhanced deposition of cigarette smoke particles in the upper respiratory tract. Aerosol Sci. Technol 2008;42:579–602.

35. Longest PW, Hindle M, Das Choudhuri S, Byron PR. Numerical simulations of capillary aerosol generation: CFD model development and comparisons with experimental data. Aerosol Sci. Technol 2007;41:952–973.

36. Longest PW, Hindle M, Das Choudhuri S, Xi J. Comparison of ambient and spray aerosol deposition in a standard induction port and more realistic mouth-throat geometry. J. Aerosol Sci 2008;39:572–591.

37. Longest PW, Hindle M, Das Choudhuri S. Effects of generation time on spray aerosol transport and deposition in models of the mouth-throat geometry. J. Aerosol Med. Pulm. Drug Deliv 2009;22(3):67–84. [PubMed: 18956949]

38. Longest PW, McLeskey JT, Hindle M. Characterization of nanoaerosol size change during enhanced condensational growth. Aerosol Sci. Technol 2010;44:473–483. [PubMed: 20640054]

39. Ma B, Lutchen KR. CFD simulations of aerosol deposition in an anatomically based human large-medium airway model. Ann. Biomed. Eng 2009;37(2):271–285. [PubMed: 19082892]

40. Martonen TB, Yang Y, Xue ZQ. Influences of cartilaginous rings on tracheobronchial fluid dynamics. Inhal. Toxicol 1994;6(3):185–198.

41. Matida EA, Finlay WH, Grgic LB. Improved numerical simulation of aerosol deposition in an idealized mouth-throat. J. Aerosol Sci 2004;35:1–19.

42. Matida EA, Finlay WH, Breuer M, Lange CF. Improving prediction of aerosol deposition in an idealized mouth using large-eddy simulation. J. Aerosol Med 2006;19(3):290–300. [PubMed: 17034305]

43. Newman, S. Respiratory Drug Delivery: Essential Theory and Practice. RDD Online; Richmond: 2009.

44. Nikander K, Prince I, Coughlin S, Warren S, Taylor G. Mode of breathing-tidal or slow and deep-through the I-neb adaptive delivery (ADD) system affects lung deposition of 99mTc-DTPA. J. Aerosol Med 2010;23(S1):S37–S43.

45. Phalen RF, Yeh HC, Schum GM, Raabe OG. Application of an idealized model to morphometry of the mammalian tracheobronchial tree. Anat. Rec 1978;190:167–176. [PubMed: 629400]

46. Robinson RJ, Russo J, Doolittle RL. 3D airway reconstruction using visible human data set and human casts with comparison to morphometric data. Anat. Rec 2009;292:1028–1044.

47. Russo J, Robinson R, Oldham MJ. Effects of cartilage rings on airflow and particle deposition in the trachea and main bronchi. Med. Eng. Phys 2008;30:581–589. [PubMed: 17719260]

48. Schroeter JD, Musante CJ, Hwang DM, Burton R, Guilmette R, Martonen TB. Hygroscopic growth and deposition of inhaled secondary cigarette smoke in human nasal pathways. Aerosol Sci. Technol 2001;34(1):137–143.

49. Smaldone GC. Advances in aerosols: adult respiratory disease. J. Aerosol Med 2006;19(1):36–46. [PubMed: 16551213]

50. Stahlhofen W, Rudolf G, James AC. Intercom-parison of experimental regional aerosol deposition data. J. Aerosol Med 1989;2(3):285–308.

51. Sung JC, Pulliam BL, Edwards DA. Nanoparticles for drug delivery to the lungs. Trends Biotechnol 2007;25:563–570. [PubMed: 17997181]

52. Vinchurkar S, Longest PW. Evaluation of hexahedral, prismatic and hybrid mesh styles for simulating respiratory aerosol dynamics. Comput. Fluids 2008;37:317–331.

53. Vinchurkar S, Longest PW, Peart J. CFD simulations of the Andersen cascade impactor: model development and effects of aerosol charge. J. Aerosol Sci 2009;40:807–822.

54. Xi J, Longest PW. Transport and deposition of micro-aerosols in realistic and simplified models of the oral airway. Ann. Biomed. Eng 2007;35(4):560–581. [PubMed: 17237991]

55. Xi J, Longest PW. Effects of oral airway geometry characteristics on the diffusional deposition of inhaled nanoparticles. ASME J. Biomech. Eng 2008;130:011008.

56. Xi J, Longest PW, Martonen TB. Effects of the laryngeal jet on nano- and microparticle transport and deposition in an approximate model of the upper tracheobronchial airways. J. Appl. Physiol 2008;104:1761–1777. [PubMed: 18388247]

57. Xie Y, Zeng P, Siegel R, Wiedmann TS, Hammer BE, Longest PW. Magnetic deposition of aerosols composed of aggregated superparamagnetic nanoparticles. Pharm. Res 2010;27(5):855–865. [PubMed: 20198407]

58. Yeh HC, Schum GM. Models of human lung airways and their application to inhaled particle deposition. Bull. Math. Biol 1980;42:461–480. [PubMed: 7378614]

59. Yin Y, Choi J, Hoffman EA, Tawhai MH, Lin C-L. Simulation of pulmonary air flow with a subject-specific boundary condition. J. Biomech 2010;43:2159–2163. [PubMed: 20483412]

60. Zhang Y, Finlay WH. Measurement of the effect of cartilaginous rings on particle deposition in a proximal lung bifurcation model. Aerosol Sci. Technol 2005;39:394–399.

61. Zhang Z, Kleinstreuer C, Kim CS. Water vapor transport and its effects on the deposition of hygroscopic droplets in a human upper airway model. Aerosol Sci. Technol 2006;40:52–67.

62. Zhang Y, Gilbertson K, Finlay WH. In vivo- in vitro comparison of deposition in three mouth-throat models with Qvar and Turbuhaler inhalers. J. Aerosol Med 2007;20(3):227–235. [PubMed: 17894531]

63. Zhang Z, Kleinstreuer C, Kim CS. Comparison of analytical and CFD models with regard to micron particle deposition in a human 16-generation tracheobronchial airway model. Aerosol Sci 2009;40:16–28.

64. Zhou Y, Cheng YS. Particle deposition in a cast of human tracheobronchial airways. Aerosol Sci. Technol 2005;39:492–500.
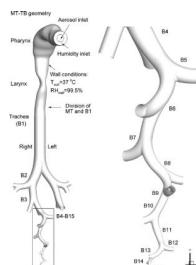
FIGURE 1.
Geometry used to evaluate the enhanced condensational growth (ECG) delivery of submicrometer aerosols in the mouth-throat (MT) and tracheobronchial (TB) regions extending down a single path to bifurcation 15 (B15) of the right lower lobe. It is noted that B11 extends behind the geometry and is therefore not visible.
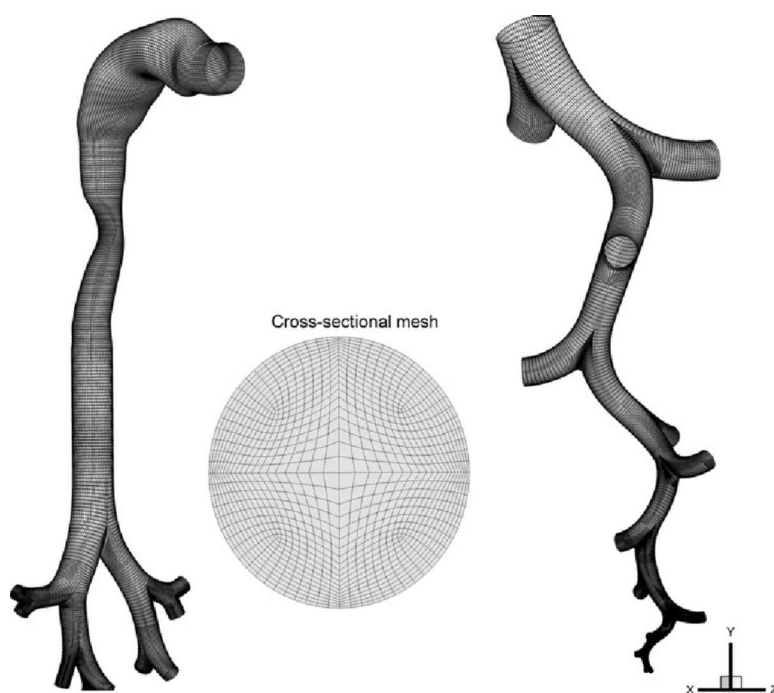
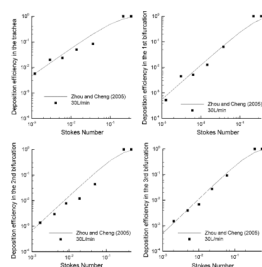Content:

FIGURE 2.
Computational mesh of the MT–TB airway model.

FIGURE 3.
Comparison of aerosol deposition efficiency in the upper TB airways between CFD predictions with the MT–TB geometry considered in this study and the experimental results of Zhou and Cheng[64] for a cast-based replica model.
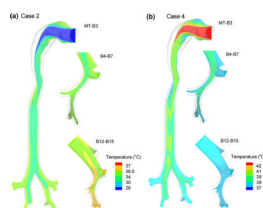
FIGURE 4.
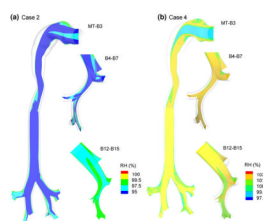Predicted temperature conditions in the MT–TB airway model for (a) Case 2 and (b) Case 4.

FIGURE 5.
Predicted relative humidity (RH) conditions in the MT–TB airway model for (a) Case 2 and (b) Case 4.
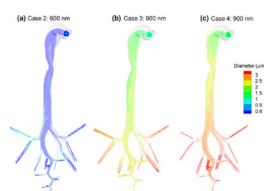
FIGURE 6.
Predicted trajectories of initially 900 nm monodisperse droplets in the MT–TB model for (a)
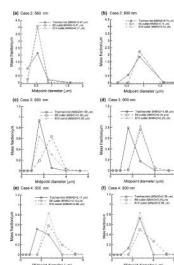Case 2, (b) Case 3, and (c) Case 4.

FIGURE 7.
CFD predictions of polydisperse size distributions at selected locations in the model for initially 560 and 900 nm monodisperse droplets and (a, b) Case 2, (c, d) Case 3, and (e, f) Case 4 delivery conditions.
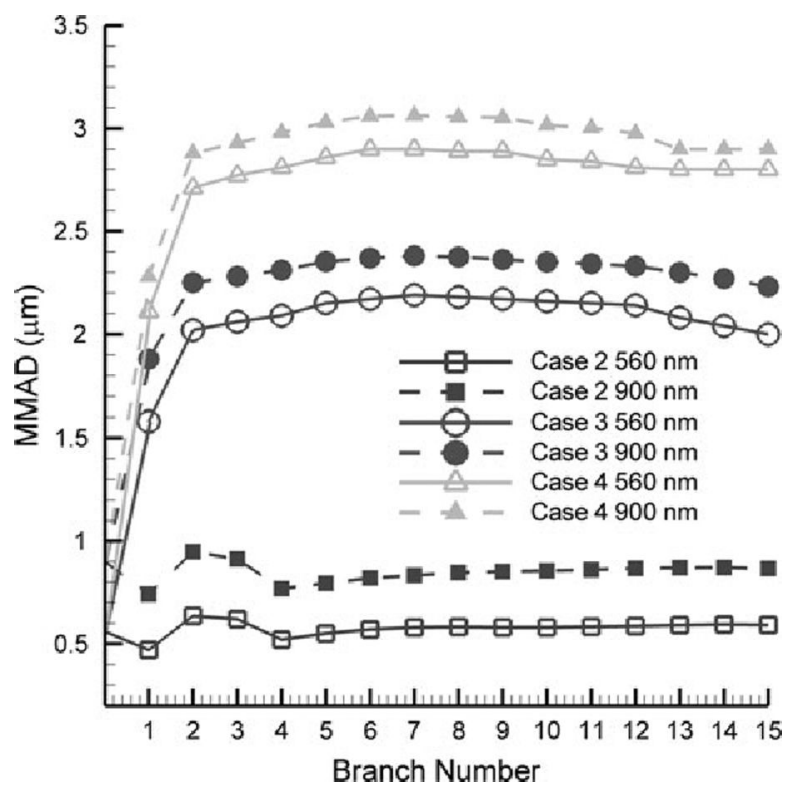
FIGURE 8.
Mass median aerodynamic diameters (MMAD) starting with the mouth inlet and entering each bifurcation from the trachea (B1) to B15 for initially 560 and 900 nm aerosols and Cases 2–4.
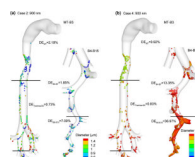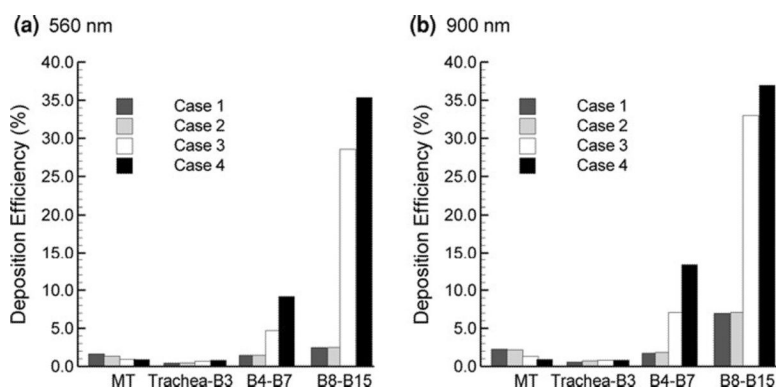
FIGURE 9.
Particle deposition locations and regional deposition efficiencies of drug mass for an initially 900 nm aerosol with (a) Case 2 and (b) Case 4 conditions.

FIGURE 10.
Comparison of deposition efficiencies (DE) within specific regions for initially (a) 560 nm and (b) 900 nm droplets and Cases 1–4.

TABLE 1

Inlet conditions for all cases considered in this study.

	Aerosol inlet	Humidified air inlet
Case 1: control; non-evaporating	Q: 9 L/min (150cm^3/s)	Q: 20 L/min (333.3 cm^3/s)
560 and 900 nm	T: 25 °C	T: 25 °C
	RH: 97.5%	RH: 50%
Case 2: control; evaporating	Q: 9 L/min (150 cm^3/s)	Q: 20 L/min (333.3 cm^3/s)
560 and 900 nm	T: 25 °C	T: 25 °C
	RH: 97.5%	RH: 50%
Case 3: ECG 1	Q: 9 L/min (150 cm^3/s)	Q: 20 L/min (333.3 cm^3/s)
560 and 900 nm	T: 39 °C	T: 39 °C
	RH: 97.5%	RH: 100%
Case 4: ECG 2	Q: 9 L/min (150 cm^3/s)	Q: 20 L/min (333.3 cm^3/s)
560 and 900 nm	T: 42 °C	T: 42 °C
	RH: 97.5%	RH: 100%

TABLE 2

Deposition efficiency (%) for each case.

	MT	Trachea-B3	B4–B7	B8–B15
Case 1				
560 nm	1.65	0.44	1.45	2.47
900 nm	2.26	0.57	1.73	6.98
Case 2				
560 nm	1.35	0.46	1.46	2.49
900 nm	2.18	0.73	1.85	7.09
Case 3				
560 nm	0.92	0.69	4.70	28.57
900 nm	1.31	0.80	7.08	33.00
Case 4				
560 nm	0.90	0.81	9.19	35.36
900 nm	0.92	0.83	13.35	36.97

TABLE 3

Comparison of deposition efficiencies with existing TB correlations.

	MMAD at the B5 outlet (μm)	Predicted DE_{TB}	DE_{TB} (Stahlhofen *et al.*[50]; Eq. 15)	DE_{TB} (Chan and Lippmann[6]; Eq. 3)
Case 1				
560 nm	0.56	0.04	0.01	0.01
900 nm	0.9	0.09	0.03	0.03
Case 2				
560 nm	0.47	0.04	0.01	0.01
900 nm	0.74	0.09	0.02	0.02
Case 3				
560 nm	2.39	0.32	0.17	0.19
900 nm	2.58	0.38	0.20	0.22
Case 4				
560 nm	3.13	0.42	0.27	0.30
900 nm	3.28	0.46	0.30	0.32

TABLE 4

Predicted pulmonary and total deposition fractions.

	MMAD at the B15 outlet (µm)	Predicted $DF_{MT\text{-}TB}$	$DF_{alveolar}$ (Stahlhofen *et al.*[50]; Eq. 19)	DF_{total}
Case 1				
560 nm	0.56	0.06	0.17	0.23
900 nm	0.9	0.11	0.27	0.38
Case 2				
560 nm	0.57	0.06	0.17	0.23
900 nm	0.84	0.11	0.26	0.37
Case 3				
560 nm	2.00	0.33	0.50	0.83
900 nm	2.23	0.39	0.52	0.91
Case 4				
560 nm	2.89	0.42	0.54	0.96
900 nm	2.95	0.46	0.54	1.00